Detailed Complementary Consistency: Wave Function Tells Particle How to Hop, Particle Tells Wave Function How to Collapse

Lei Huang, *Zhecun Shi*, *and Linjun Wang**

Key Laboratory of Excited-State Materials of Zhejiang Province, Department of Chemistry, Zhejiang University, Hangzhou 310058, China

ABSTRACT: In mixed quantum-classical dynamics, the time evolution of the quantum subsystem can involve both wave function and particle-like descriptions, which may yield inconsistent results for the expectation value of the same physical quantity. In this study, we propose a novel detailed complementary consistency (DCC) method, which achieves fully consistent results based only on the principle of internal consistency in nonadiabatic dynamics. Namely, wave function tells particle how to hop along each trajectory, while particle tells wave function how to collapse based on the occupation of active states. As benchmarked in a diverse array of representative models, DCC not only gives identical populations based on both wave functions and active states, but also closely and systematically reproduces the exact quantum dynamics. Due to the high performance, our new DCC method provides a promising approach toward more consistent mixed quantum-classical description of nonadiabatic dynamics with much better reliability and efficiency for general applications.

In chemistry, physics, biology, and materials science, many important processes (e.g. proton transfer[1,2], charge transport[3,4], exciton diffusion[5,6], energy relaxation[7,8], and singlet fission[9,10]) all belong to the category of nonadiabatic dynamics. Due to the presence of quantum transitions, the traditional Born-Oppenheimer approximation is no longer valid, and the electronic and nuclear dynamics are strongly coupled. To accurately simulate these processes, different quantum dynamics methods have been proposed, including, for instance, the multiconfigurational time-dependent Hartree (MCTDH)[11,12], the time-dependent density matrix renormalization group (TD-DMRG)[13,14], and the hierarchical equations of motion (HEOM)[15,16]. Despite the great successes, fully quantum dynamics generally needs high computational cost, which has significantly limited their applications in nonadiabatic dynamics problems of large complex systems.

Mixed quantum-classical dynamics has emerged as a promising alternative to fully quantum dynamics for studying complex nonadiabatic processes[17,18]. We may consider a general system with both electronic and nuclear degrees freedom, whose coordinates are **r** and **x**, respectively. At each time *t* along each trajectory *j*, the nuclear coordinates are given by $\mathbf{x}_j(t)$ and the electronic wave function $\left|\psi_j(\mathbf{r},t)\right\rangle$ reads

$$\left|\psi_j(\mathbf{r},t)\right\rangle = \sum_j w_i^j(t)\left|\phi_i(\mathbf{r})\right\rangle, \tag{1}$$

where $\left|\phi_i(\mathbf{r})\right\rangle$ is the electronic basis for state *i*. In a mixed quantum-classical manner, the nuclei move classically and the electron is propagated quantum mechanically along the trajectory. As a result, the wave function description for the population distribution on electronic state *i* at position **x** is given by[19]

$$\rho_{ii}^{\mathrm{wf}}(\mathbf{x},t)=\frac{1}{N}\sum_{j}\left|w_i^j(t)\right|^2\delta(\mathbf{x}-\mathbf{x}_j(t))\,, \tag{2}$$

where N is the number of trajectories. To give a particle-like description of the same distribution, we also assume that each trajectory j occupies an active electronic state $a_j(t)$ at time t. Then, the population distribution can be calculated by the probability that a trajectory stays at the specific position $\mathbf{x}$ and state i,

$$\rho_{ii}^{\mathrm{as}}(\mathbf{x},t)=\frac{1}{N}\sum_{j}\delta_{i,a_j(t)}\delta(\mathbf{x}-\mathbf{x}_j(t))\,. \tag{3}$$

In principle, these two descriptions should yield identical results because they represent different interpretations of the same population distribution. In the discussions below, this is referred to as the principle of internal consistency.

As a seminal mixed quantum-classical dynamics method, Tully's fewest switches surface hopping (FSSH)[20] has been widely utilized in many different fields. However, the standard FSSH does not guarantee the internal consistency due to the presence of frustrated hops and lack of decoherence[21-24]. Recently, we proposed the auxiliary branching corrected surface hopping (A-BCSH)[25] method, which achieved much better accuracy and consistency simultaneously compared to FSSH. In addition, by introducing the particle-like description to the Ehrenfest mean field (EMF)[26] dynamics, the auxiliary branching corrected mean field (A-BCMF)[27] method not only gives correct channel populations but also captures the time-dependent spatial distribution of population. Both of these two auxiliary trajectory methods indicate an underlying connection between accuracy and internal consistency in mixed quantum-classical dynamics.

When inconsistency arises, equating $\rho_{ii}^{\mathrm{wf}}(\mathbf{x},t)$ and $\rho_{ii}^{\mathrm{as}}(\mathbf{x},t)$ cannot be directly carried out due to the ambiguity regarding the accuracy of these two quantities. To solve this problem, we can apply the consistency correction in some order. On one side, the wave function propagation follows the time-dependent Schrödinger equation (TDSE), giving the first-order derivative of population with respect to time and defining the population fluxes between any two states. These population fluxes cannot be directly obtained by the particle-like description based on active states, in which the trajectories move on adiabatic potential energy surfaces (PESs) by classical dynamics. Thereby, it is natural to use these fluxes to redistribute occupation of active states, which ensures the unidirectional consistency from wave function to particle-like descriptions. Namely, wave function tells particle how to hop, just as in the traditional FSSH. On the other side, the classical nuclear dynamics conserves the total energy and gives the reliable spatial distribution[28,29]. In comparison, the wave function evolution could increase the population of a specific state with higher energy than the total energy. Thereby, using active states to guide the wave function collapse also helps to achieve the internal consistency between wave function and particle-like descriptions. The surface hops do not directly impact the spatial distribution, and thus should be made prior to the wave function collapse. As a result, the internal consistency is realized for population distributions in both the nuclear phase space and the electronic state space.

Based on the internal consistency, a general detailed complementary consistency (DCC) method is given below. The total Hamiltonian can be written as

$$\hat{H} = \hat{T}_n + \hat{H}_e(\mathbf{r};\mathbf{x}), \tag{4}$$

where $\hat{T}_n$ represents the kinetic energy operator of the nuclei, and $\hat{H}_e(\mathbf{r};\mathbf{x})$ is the electronic Hamiltonian operator at the given nuclear position **x**. By solving the time-independent Schrödinger equation,

$$\hat{H}_e(\mathbf{r};\mathbf{x})\left|\phi_i(\mathbf{r};\mathbf{x})\right\rangle = E_i(\mathbf{x})\left|\phi_i(\mathbf{r};\mathbf{x})\right\rangle, \tag{5}$$

we can get the adiabatic energies $E_i(\mathbf{x})$ and the corresponding orthonormal adiabatic states $\left\{\left|\phi_i(\mathbf{r};\mathbf{x})\right\rangle\right\}$. The electronic wave function $\left|\psi(\mathbf{r})\right\rangle$ can be linearly expanded as

$$\left|\psi(\mathbf{r})\right\rangle = \sum_i c_i \left|\phi_i(\mathbf{r};\mathbf{x})\right\rangle, \tag{6}$$

where c_i are the expansion coefficients. Substituting Eq. (6) into the TDSE results in

$$i\hbar\frac{d}{dt}c_i = \sum_j c_j\left(V_{ij} - i\hbar\dot{\mathbf{x}}\cdot\mathbf{d}_{ij}\right), \tag{7}$$

where $V_{ij} = \left\langle\phi_i(\mathbf{r};\mathbf{x})\,|\,\hat{H}_e(\mathbf{r};\mathbf{x})\,|\,\phi_j(\mathbf{r};\mathbf{x})\right\rangle$ are the matrix elements of the adiabatic Hamiltonian and $\mathbf{d}_{ij} = \left\langle\phi_i(\mathbf{r};\mathbf{x})\,|\,\nabla_{\mathbf{x}}\phi_j(\mathbf{r};\mathbf{x})\right\rangle$ are the nonadiabatic couplings (NACs) between adiabatic states *i* and *j*. The time evolution of the density matrix element $\rho_{ij} = c_i c_j^*$ along the trajectory is then given by

$$i\hbar\frac{d}{dt}\rho_{ij} = \sum_k\left[\rho_{kj}\left(V_{ik} - i\hbar\dot{\mathbf{x}}\cdot\mathbf{d}_{ik}\right) - \rho_{ik}\left(V_{kj} - i\hbar\dot{\mathbf{x}}\cdot\mathbf{d}_{kj}\right)\right]. \tag{8}$$

The nuclei are evolved on the active PES *a* through the Newtonian equation

$$\frac{d\mathbf{p}}{dt} = -\nabla_{\mathbf{x}}V_{aa}, \tag{9}$$

where **p** represents the nuclear momenta.

In principle, different approaches exist to ensure the consistency of active states based on the wave function. For instance, surface hopping probabilities can be defined based on NACs as in FSSH[20] and global fluxes as in the global flux surface hopping (GFSH)[28]. Recently, we have shown that both FSSH and GFSH with proper branching correction gives identical results in multilevel scattering systems[31]. In addition, this

consistency correction can be realized via either coupled or independent trajectories. For simplicity, we here adapt the FSSH hopping probabilities and use velocity rescaling along the NAC direction for successful surface hops to conserve the total energy.

Considering the consistency correction to the wave function based on active states, each trajectory has the corresponding wave function, the total number of wave function variables is larger than the total count of linear equations. Thereby, there also exist a variety of potential solutions for the correction. In this study, we propose the simplest approach. In detail, the diagonal elements of the density matrix ρ'_{ii} is set as

$$\rho'_{ii} = \rho^{\mathrm{as}}_{ii}\,, \tag{10}$$

where ρ^{as}_{ii} represents the local occupancy of active states. Subsequently, we rescale the off-diagonal density matrix elements by

$$\rho'_{ij} = \frac{\sqrt{\rho'_{ii}\rho'_{jj}}}{|\,\rho_{ij}\,|}\rho_{ij}\,, \tag{11}$$

where ρ_{ij} and ρ'_{ij} represent off-diagonal elements of the density matrix before and after the consistency correction, respectively.

Suppose the nuclear coordinates and momenta along each trajectory *i* at time *t* are given by $\mathbf{x}_i(t)$ and $\mathbf{p}_i(t)$, respectively. For a specified trajectory *i*, we determine the number of local neighbors on each PES *l* within a specified distance ε whose directions of momenta are within a specified angular distance θ,

$$N_l^i = \sum_{j=1}^{N} \Theta\left(\varepsilon^2 - \|\,\mathbf{x}_i - \mathbf{x}_j\,\|^2\right)\Theta\left(\frac{\mathbf{p}_i\cdot\mathbf{p}_j}{\|\,\mathbf{p}_i\,\|\cdot\|\,\mathbf{p}_j\,\|} - \cos(\theta)\right)\delta_{l,a_j}\,, \tag{12}$$

where a_j is the active state of trajectory *j*, $\|\cdot\|$ represents the Euclidean norm, and $\Theta(x)$ is the Heaviside step function defined as

$$\Theta(x)=\begin{cases}1, & x\geq 0\\ 0, & x<0\end{cases}. \tag{13}$$

Given Eq. (12), we can estimate the local trajectory density for the l-th trajectory as

$$\rho_{ll}^{i,\mathrm{as}}=\frac{N_l^i}{\sum_l N_l^i}. \tag{14}$$

Here, we have introduced the parameters ε and θ to estimate the number of trajectories within a local range to a specified trajectory, which significantly enhance the numerical stability and efficiency.

To benchmark the performance of DCC, we here investigate a variety of two-level models, which have been extensively studied in the literature. Atomic units are used unless otherwise noted. We first focus on three one-dimensional standard scattering models proposed by Tully[20], including the simple avoided crossing (SAC), the dual avoided crossing (DAC), the extended coupling with reflection (ECR) models. We then study two more challenging two-dimensional scattering models proposed by Subotnik[32,33], i.e., STD-1 and STD-2 models. Finally, we consider three one-dimensional bound-state models proposed by Agostini[34,35], i.e., BS-1, BS-2 and BS-3 models. Using the exact quantum dynamics by the discrete variable representation (DVR)[36] method as references and the FSSH results for comparison, we reveal the universal applicability of DCC. To check the internal consistency, the DCC (FSSH) results based on active states and wave functions are named as DCC-as and DCC-wf (FSSH-as and FSSH-wf), respectively.

In Figure 1A, we show the channel population of transmission on the upper PES as a function of the initial momentum k in the SAC model. While FSSH-as properly characterizes the dynamics, FSSH-wf performs well only for $k>10$. In the small k cases,

many trajectories do not have enough kinetic energies to hop to the upper state in the interacting region, leading to frustrated hops and inconsistency between active states and wave functions. As these trajectories leave the interacting region, the wave function calculated by TDSE still contributes to transmission on the upper PES, while the active states do not have such probabilities. Due to the inherent internal consistency, DCC naturally solves these issues. Regardless of the analysis method, both DCC-as and DCC-wf consistently reproduce the exact quantum dynamics. Figure 1B shows strong Steuckelberg oscillations in the transmission on the upper PES in the DAC model due to quantum interference. Compared with the exact quantum solutions, FSSH shows smaller oscillation amplitudes and different phases. Again, FSSH-as and FSSH-wf give inconsistent results for small k. In contrast, DCC gives fully consistent results and more closely reproduces the exact quantum dynamics.

In Figures 1C and 1D, we study reflection on the lower PES and transmission on the upper PES in the ECR model, respectively. It is apparent that FSSH shows even more significant inconsistency. In high k cases, both DCC and FSSH agree well with the quantum dynamics. In principle, when the kinetic energies are not enough to afford surface hops to the upper PES, there should be no transmission on the excited PES. For small k, the FSSH-as and FSSH-wf results diverge from each other, with evident oscillations and overestimated strengths in the reflection probabilities on the lower PES. The inconsistent FSSH trajectories become more problematic when they re-enter the interaction region, leading to wrong population fluxes and errors in the reflection channel. In comparison, DCC always maintains the consistency, ensuring accurate

fluxes even when multiple interaction regions are present. These results highlight the importance of consistency in complex systems.

Besides the final channel populations, we also examine the spatial distribution of population at different time to further benchmark the performance of FSSH and DCC. As an illustration, we consider the ECR model with the initial $k = 10$. Figure 2 illustrates three critical snapshots of the dynamics, i.e., entry of the initial wave packet into the interaction region, reflection of the wave packet on the upper PES due to insufficient kinetic energy, and reentry of the reflected wave packet into the interaction region. In the ECR model, the absence of significant splitting in the adiabatic potential energies within the interaction region allows the trajectories to have enough energy for surface hops, resulting in relatively consistent performance of FSSH in the first snapshot. As a result, both FSSH and DCC produce the spatial distributions of population that agree well with the exact quantum dynamics regardless of the trajectory analysis approach (see Figures 2A and 2D). However, inconsistency emerges in FSSH-as and FSSH-wf results when the wave packets exit the interaction region and branch on different PESs (see Figures 2B and 2E). In particular, FSSH-wf underestimates (overestimates) the population of the upper (lower) state for $x < -1.5$, and it is the opposite for $x > 1.5$. As shown in Figures 2C and 2F, the inconsistency of FSSH results in inaccurate transitions upon re-entering the interaction region, significantly deviating from the exact quantum dynamics. Encouragingly, DCC consistently reproduces the correct spatial distributions of population throughout the simulation.

In the one-dimensional scattering models studied above, DCC has demonstrated

consistency and high accuracy simultaneously. We further investigate whether the DCC method can effectively describe more complex problems involving more classical degrees of freedom. We consider two representative models proposed by Subotnik. The Hamiltonian of the STD-1 model is defined by

$$H_{11}(x,y) = -A_1 \tanh(B_1 x), \tag{15}$$

$$H_{22}(x,y) = A_2 \tanh[B_2(x-1) + C_2 \cos(D_2 y + \pi/2)] + 3A_2/4, \tag{16}$$

$$H_{21}(x,y) = A_3 \exp(-B_3 x^2), \tag{17}$$

where A_1 = 0.05, B_1 = 0.6, A_2 = 0.2, B_2 = 0.6, C_2 = 2.0, D_2 = 0.3, A_3 = 0.015, and B_3 = 0.3. In the original study of Subotnik, an initial Gaussian wave packet is placed on the upper surface at (x_0, y_0) where x_0 = -4.0 and y_0 ranges in -2.0, -1.0, 0.0, 1.0 and 2.0. To assess the performance of our DCC method across a broader range of parameters, we here expand the range of (x_0, y_0) for the initial wave packet. Namely, x_0 still takes the value of -4.0, but y_0 now spans in -2.0, -1.0, 0.0, 1.0, 2.0, 3.0, 4.0, 5.0, and the initial momentum is oriented at angles of 15, 30, and 45 degrees relative to the x-axis. The wave packet is placed on either the adiabatic ground state or excited state. When the initial wave packet is on the ground (excited) state, the momenta range from 8 to 20 (4 to 16). We use a time step of dt = 0.2 and obtain a snapshot every 500 time steps. The boundaries are set from -15 to 15. For each set of initial parameters, the maximum simulation time for the dynamics corresponds to the time at which the electronic population of 10^{-6} passes through the boundary in exact quantum dynamics. The entire space is divided by two central lines (i.e., x = 0 and y = 0) into four sections. This division, along with the incorporation of two electronic states, results in a total number

of eight channels. The population of each channel is calculated by integrating the electronic population density within the corresponding channel.

In Figure 3, we show the root mean square errors (RMSE) in channel populations at the final snapshot for different initial conditions. The RMSE is defined as

$$\mathrm{RMSE} = \sqrt{\frac{1}{8}\sum_{j=1}^{M}\sum_{i=1}^{8}\left(P_i^{\mathrm{method,j}} - P_i^{\mathrm{DVR,j}}\right)^2}, \tag{18}$$

where M represents the number of total initial conditions, $P_i^{\mathrm{method},j}$ is the population of the i-th channel for the j-th initial condition by a surface hopping method. The RMSE quantifies the average error between the results of a method and the exact quantum solutions, providing a comprehensive measure of accuracy in predicting channel populations for a large range of initial conditions.

Figures 3A and 3B show notable RMSE differences between the FSSH-as and FSSH-wf results with a value of about 0.09. This divergence points to a considerable inconsistency in FSSH. Even when employing the active states for analysis, the error remains at about 0.03. This higher error mirrors the similar challenges seen in the ECR model. A key issue arises after the wave packet encounters steep PESs, leading to a significant divergence between the results based on active states and wave functions, primarily due to the branching of wave packets. In addition, cumulative errors manifest when the wave packet reenters the interaction region. In contrast, the DCC method is free from these complications. By consistently holding the internal consistency, it avoids the error caused by wave packet branching and frustrated hopping, significantly reducing the errors to about 0.01, a substantial reduction of nearly two-thirds. Notably, both trajectory analysis methods produce identical results with DCC.

The Hamiltonian of the STD-2 model is defined by

$$H_{11}(x,y) = -E_0\,, \tag{19}$$

$$H_{22}(x,y) = -A\exp\left(-B\left(0.75(x+y)^2 + 0.25(x-y)^2\right)\right), \tag{20}$$

$$H_{12}(x,y) = H_{21}(x,y) = C\exp\left(-D\left(0.25(x+y)^2 + 0.75(x-y)^2\right)\right), \tag{21}$$

where A = 0.15, B = 0.14, C = 0.015, D = 0.06, and E_0 = 0.05. In conducting a thorough evaluation of FSSH and DCC, we established initial conditions with x_0 = -8 and y_0 varying from -2 to 5 and altered the angle θ at intervals of 0°, 15°, 30°, and 45° relative to the x-axis. An initial wave packet is placed either on the adiabatic ground state or the excited state. When initiating from the ground (excited) state, the momenta range from 16 to 28 (8 to 20). As a result, we analyzed the channel populations over a comprehensive set of 832 initial conditions calculated by the FSSH and DCC methods based on the two distinct analysis strategies. The time step size is fixed at dt = 0.2, with x-axis boundaries from -15.0 to 25.0 and y-axis boundaries from -15.0 to 25.0. The definition of channel populations is consistent with that in STD-1.

As shown in Figures 3C and 3D, FSSH-as and FSSH-wf produce inconsistent results, with errors about 0.04 when compared to the exact quantum dynamics. In contrast, DCC-as and DCC-wf yield identical results, consistently reducing the error for each initial momentum to approximately 0.01. As a result, this represents a substantial reduction of nearly 75% in error. These results further suggest that ensuring the internal consistency between occupation of active states and population based on wave functions can significantly reduce the errors inherent in FSSH. As a result, the DCC method not only provides qualitatively accurate results but also achieves smaller

quantitative errors, enhancing the overall reliability and precision.

We further select an initial condition for the STD-2 model where the trajectory starts from the excited state with initial parameters x = -8, y = 0, θ = 15° and k = 16. In Figures 4a and 4b, we show the population distributions of the excited and ground states at the final snapshot t = 1900 au. As the initial wave packet enters the interaction region from the left, a new wave packet component is formed on the excited PES due to the NAC. These wave packets branch in the interaction region. While the initial wave packet remains in this region, it spawns another wave packet on the ground PES. However, because the interaction is not strong at the edge of the interaction region, the intensity of the new wave packet is relatively weak. At the final moment, the wave packets are completely separated, resulting in two primary population channels and a secondary population channel. It is apparent that the FSSH population distribution based on wave functions shows wrong numbers of wave packets on both the ground and excited PESs. In contrast, DCC successfully reproduces both the shape and peak intensity of the exact quantum dynamics. This further demonstrates the accuracy of DCC in handling branching within the interaction region.

To further examine the performance of DCC in condensed phase systems, we consider a one-dimensional bound-state model, which consists of one nuclear degree of freedom and two electronic states. The Hamiltonian is given by

$$H_{11}(x) = \frac{1}{2}k(R - R_1)^2, \tag{22}$$

$$H_{22}(x, y) = \frac{1}{2}k(R - R_2)^2 + \Delta, \tag{23}$$

$$H_{12} = H_{21} = be^{-a(R-R_3)^2}, \tag{24}$$

where $k = 0.02$, $a = 3.0$, $R_1 = 6.0$ and $R_2 = 2.0$. We consider different energy difference Δ and reorganization energy $E_r = k(R_1 - R_2)^2 / 2$. BS-1 and BS-3 are in the direct regime and BS-2 is in the inverted regime. The other parameters are listed in the Supporting Information. In BS-1 and BS-2, the initial wave packets are fully promoted to the excited state. In BS-3, however, 20% of the probability density gets vertically promoted to the excited state creating a coherent superposition to mimic the effect of a short laser and the wave packet is simulated from this state with the field turned off.

The excited state populations can be calculated as

$$\rho_{22}^{\text{as}}(t) = \frac{1}{N}\sum_j \delta_{2,a_j(t)}\,, \tag{25}$$

$$\rho_{22}^{\text{wf}} = \frac{1}{N}\sum_j \left|w_2^j(t)\right|^2\,. \tag{26}$$

With the population distributions in Eq. (2), we can define the coherence as

$$\sigma_{12}(t) = \int \mathrm{d}\mathbf{x}\, \frac{\rho_{11}(\mathbf{x},t)\rho_{22}(\mathbf{x},t)}{\rho_{11}(\mathbf{x},t) + \rho_{22}(\mathbf{x},t)}\,, \tag{27}$$

which indicates the intensity of overlap for the wave packets.

As shown in Figure 5, the excited-state population in the exact quantum dynamics experiences stepwise transitions to the ground state, as the nuclear wave packet periodically evolves through the crossing region. And the coherence shows periodic increase and subsequent decay to zero because of the reflection and separation of wave packets on different surfaces. In all the three investigated bound-state models under various parameters and initial conditions, DCC shows accurate and consistent results between occupation of active states and population based on wave functions. Conversely, the FSSH method yields inconsistent and inaccurate results. As shown in

Figure 5E, the wave functions in FSSH even erroneously give an increase in the population of the excited state. In addition, FSSH-as overestimates the population transfer from the excited state to the ground state due to the lack of decoherence, leading to substantial deviations from the exact quantum dynamics. The shortcomings of FSSH become more pronounced when its inconsistent wave functions are used in coherence calculations. As shown in Figures 5B, 5D and 5F, the wave functions remain coherent after the first coherent event. In comparison, DCC successfully captures the decoherence by the exact quantum dynamics.

Finally, there are still a few points worth discussing. (1) In principle, multiple potential solutions are present to ensure the consistency between active states and wave functions. For clarity, we adopt the simplest approach in the present study, wherein the population of each state for any trajectory follows the local occupation of active states. The principle of internal consistency can be also realized by solving more equations. (2) In this study, the DCC algorithm relies solely on the local occupation of active states, which can be regarded as the local trajectory density approximation. We have shown that even this approximation could give encouraging results. Advanced corrections could be implemented by considering the spatial gradient or higher-order derivatives of the trajectory density to consider non-local effects. (3) The number of trajectories needed for direct DCC simulations increases with the spatial dimensionality. To consider the internal consistency principle for general condensed matter systems (e.g., the Fenna-Mathews-Olson complex[37] and the spin-boson models[38-40]), efficient strategies are required to reduce the number of trajectories. These studies are currently

under way.

In summary, we have proposed the principle of internal consistency for results based on wave functions and active states to reproduce the exact quantum results. Based on this principle, we have presented a novel DCC method for mixed quantum-classical dynamics. This involves surface hops and wave function collapse based on the occupation of active states from the neighboring trajectories. DCC has been extensively benchmarked in both one-dimensional and two-dimensional systems. The results have consistently exhibited high accuracy, regardless of whether the active states or wave functions are used for trajectory analysis. The remarkable accuracy achieved by DCC presents significant potential for its application in general complex nonadiabatic problems. From some point of view, our DCC method can be regarded as a self-consistent description of the wave-particle duality and deserves further study.

AUTHOR INFORMATION

Corresponding Author

*Email: ljwang@zju.edu.cn

ORCID

Linjun Wang: 0000-0002-6169-7687

Author Contributions

The manuscript was written through contributions of all authors. All authors have given approval to the final version of the manuscript.

Notes

The authors declare no competing financial interests.

ACKNOWLEDGMENTS

L.W. acknowledges support from the National Natural Science Foundation of China (Grant No. 22273082) and the High-Performance Computing Center in Department of Chemistry, Zhejiang University.

ASSOCIATED CONTENT

Supporting Information

We give the computational details, parameter convergence of the DCC results, and additional results for the two-dimensional models.

This information is available free of charge online.

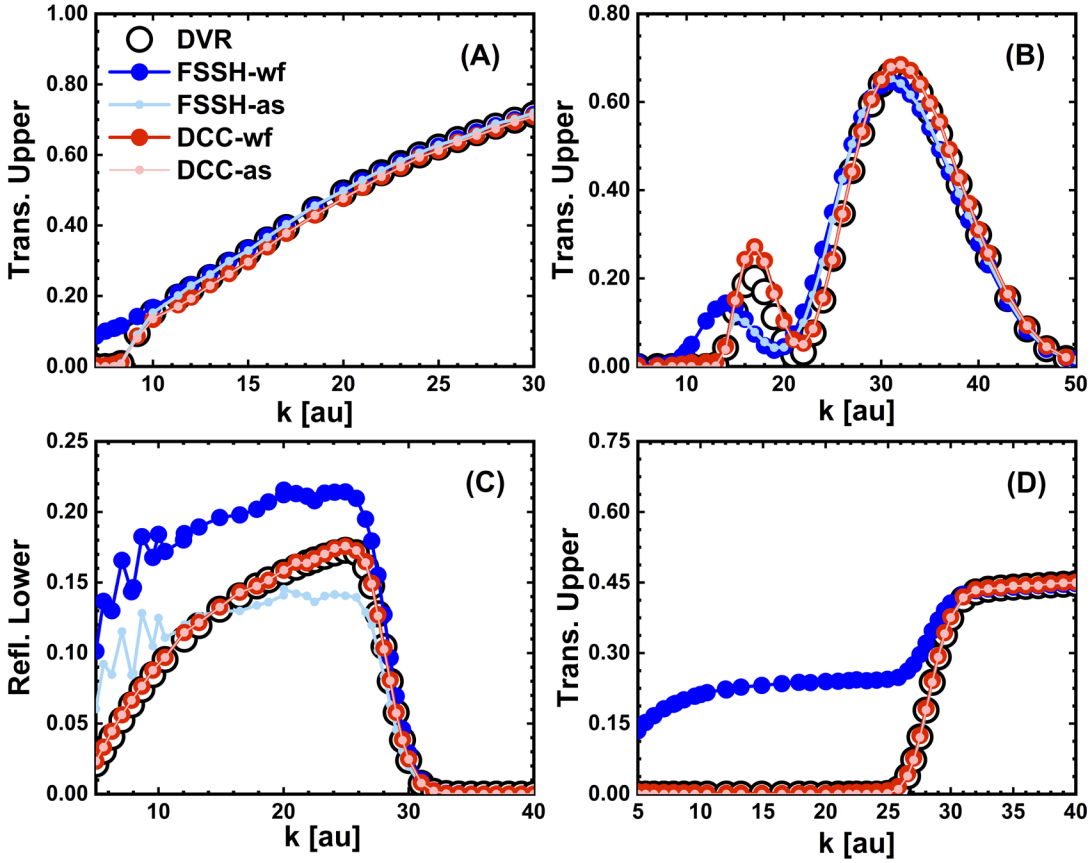

Figure 1. Transmission probabilities on the upper surface for (A) SAC and (B) DAC models, and (C) reflection probabilities on the lower surface and (D) transmission probabilities on the upper surface for the ECR model. The black open circles represent the exact quantum dynamics by DVR. The results of FSSH-as, FSSH-wf, DCC-as and DCC-wf are shown by light blue, blue, light red and red solid circles, respectively.

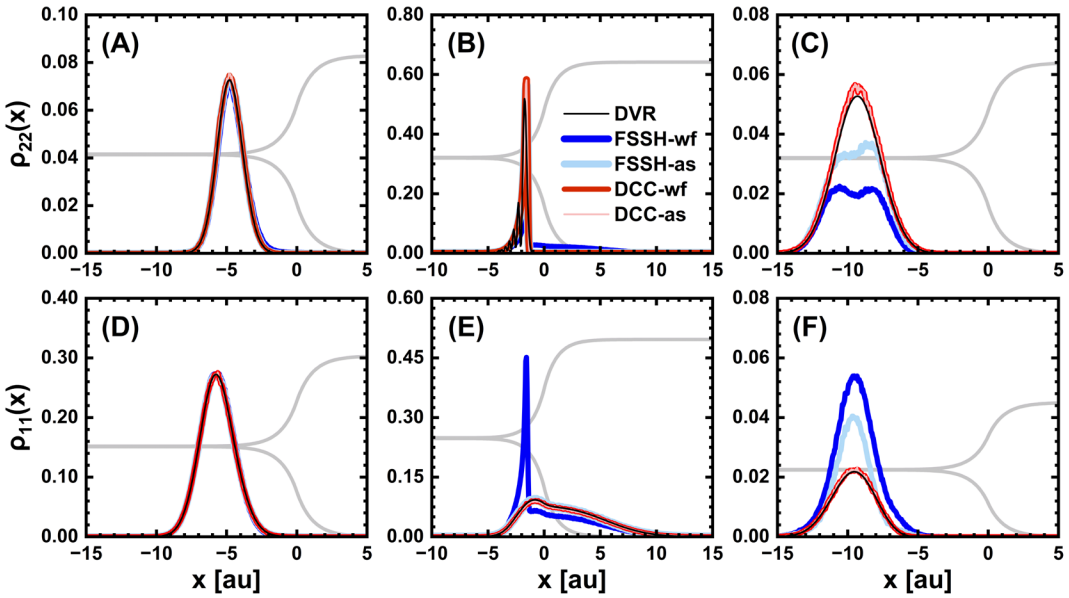

Figure 2. Population distributions on the (A-C) upper and (D-F) lower surfaces for the ECR model with the initial momentum of k = 10 au. The black lines represent the exact quantum dynamics by DVR. The results of FSSH-as, FSSH-wf, DCC-as and DCC-wf are shown by light blue, blue, light red, and red lines, respectively. The upper and lower adiabatic PESs are shown by grey lines. (A, D), (B, E) and (C, F) correspond to t = 3000, 4000 and 6000 au, respectively.

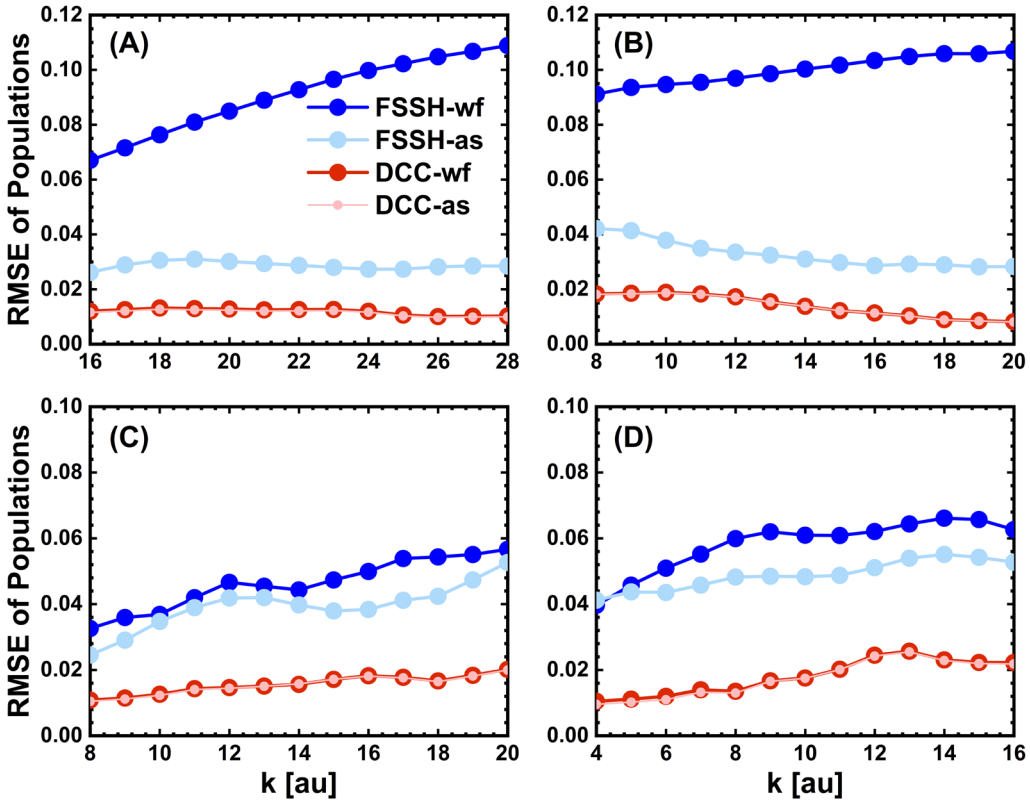

Figure 3. RMSE of populations for the STD-1 model when initially starting from the (A) lower and (B) upper surfaces, and RMSE of populations for the STD-2 model when initially starting from the (C) lower and (D) upper surfaces. The results of FSSH-as, FSSH-wf, DCC-as and DCC-wf are shown by light blue, blue, light red and red solid circles, respectively.

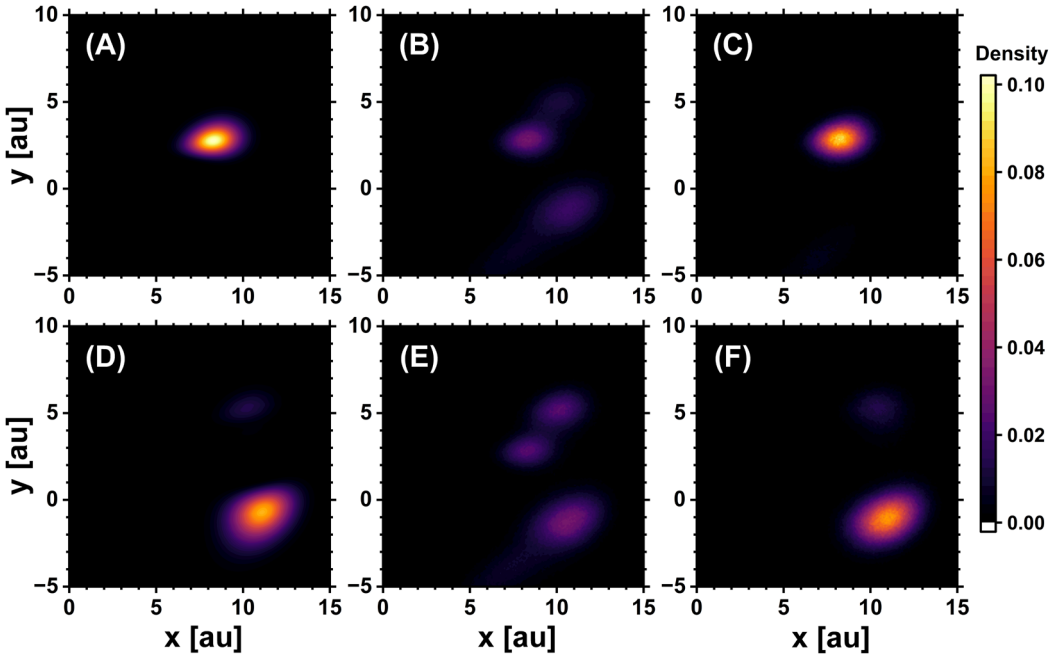

Figure 4. Spatial distribution of population for the STD-2 model on the (A-C) upper and (D-F) lower surfaces at t = 1900 au. The initial wave packet is placed on the upper surface with the parameters x = -8, y = 0, θ = 15° and k = 16. (A, D), (B, E) and (C, F) correspond to the exact quantum dynamics by DVR, the results by FSSH-wf and DCC-wf, respectively. The lighter colors indicate higher populations.

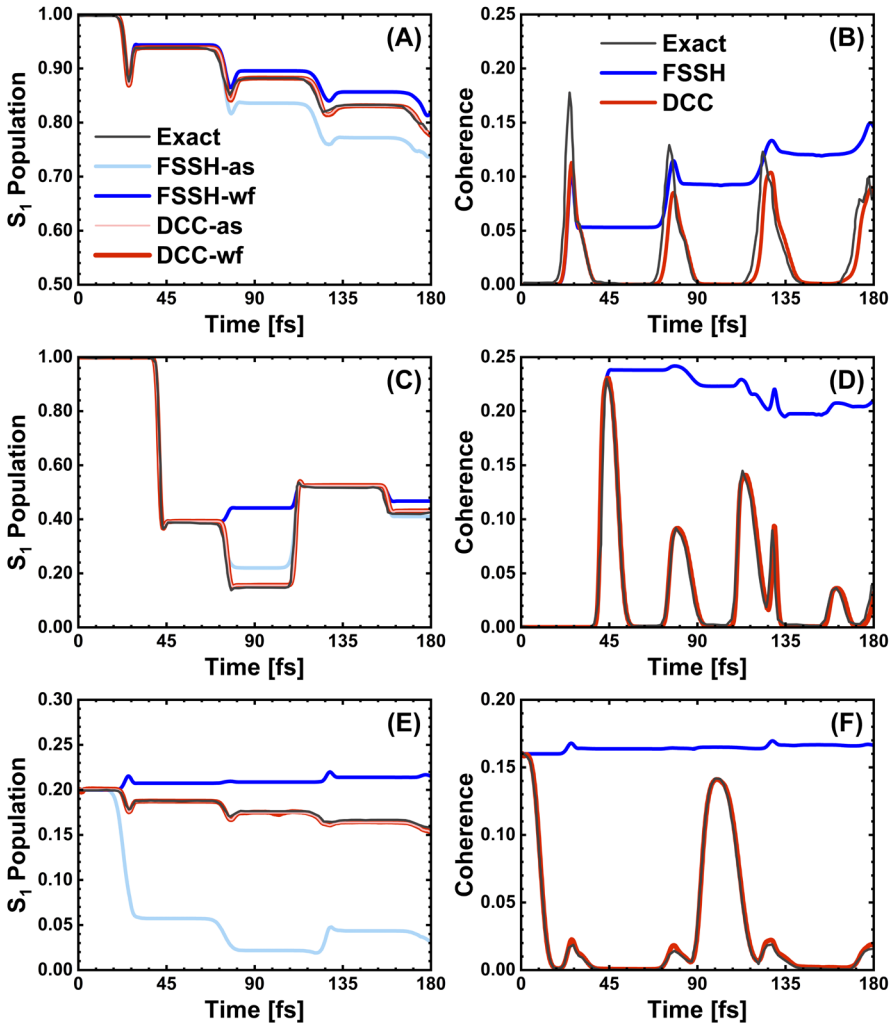

Figure 5. Time-dependent population of the excited-state population and coherence for the (A, B) BS-1, (C, D) BS-2 and (E, F) BS-3 models. The black lines represent the exact quantum dynamics. In (A, C, E), the results of FSSH-as, FSSH-wf, DCC-as and DCC-wf are shown by light blue, blue, light red and red lines, respectively. In (B, D, F), the results of FSSH and DCC are shown by blue and red lines, respectively.

REFERENCE

(1) Bourne-Worster, S.; Worth, G. A. Quantum Dynamics of Excited State Proton Transfer in Green Fluorescent Protein. *J. Chem. Phys.* **2024**, 160, 065102.

(2) Codescu, M.-A.; Kunze, T.; Weiß, M.; Brehm, M.; Kornilov, O.; Sebastiani, D.; Nibbering, E. T. J. Ultrafast Proton Transfer Pathways Mediated by Amphoteric Imidazole. *J. Phys. Chem. Lett.* **2023**, 14, 4775–4785.

(3) Oberhofer, H.; Reuter, K.; Blumberger, J. Charge Transport in Molecular Materials: An Assessment of Computational Methods. *Chem. Rev.* **2017**, 117, 10319–10357.

(4) Geng, H.; Zhu, L.; Yi, Y.; Zhu, D.; Shuai, Z. Superexchange Induced Charge Transport in Organic Donor–Acceptor Cocrystals and Copolymers: A Theoretical Perspective. *Chem. Mater.* **2019**, 31, 6424–6434.

(5) Takabayashi, Y.; Sato, H.; Higashi, M. Theoretical Analysis of the Coordination-State Dependency of the Excited-State Properties and Ultrafast Relaxation Dynamics of Bacteriochlorophyll a. *Chem. Phys, Lett.* **2023**, 826, 140669.

(6) De, P. K.; Jain, A. Metal-Induced Fast Vibrational Energy Relaxation: Quantum Nuclear Effects Captured in Diabatic Independent Electron Surface Hopping (IESH-D) Method. *J. Phys. Chem. A* **2023**, 127, 4166–4179.

(7) Sneyd, A. J.; Beljonne, D.; Rao, A. A New Frontier in Exciton Transport: Transient Delocalization. *J. Phys. Chem. Lett.* **2022**, 13, 6820–6830.

(8) Liu, J.; Zhang, X.; Lu, G. Non-Adiabatic Exciton Dynamics in van Der Waals Heterostructures. *J. Phys. Chem. Lett.* **2022**, *13* (50), 11760–11769.

(9) Barford, W.; Chambers, C. A. Theory of Singlet Fission in Carotenoid Dimers. *J.Chem. Phys.* **2023**, 159, 084116.

(10) López-Carballeira, D.; Polcar, T. Singlet Fission Driven by Excited-State Intramolecular Proton Transfer (ESIPT+SF): A (TD)DFT Study. *ChemPhotoChem* **2023**, 7, e202300017.

(11) Beck, M. H.; Jäckle, A.; Worth, G. A.; Meyer, H.-D. The Multiconfiguration Time-Dependent Hartree (MCTDH) Method: A Highly Efficient Algorithm for Propagating Wavepackets. *Physics Reports* **2000**, 324, 1–105.

(12) Wang, H.; Thoss, M. Multilayer Formulation of the Multiconfiguration Time-Dependent Hartree Theory. *J. Chem. Phys*. **2003**, 119, 1289–1299.

(13) White, S. R. Density Matrix Formulation for Quantum Renormalization Groups. *Phys. Rev. Lett.* **1992**, 69, 2863–2866.

(14) Ren, J.; Li, W.; Jiang, T.; Wang, Y.; Shuai, Z. Time-Dependent Density Matrix Renormalization Group Method for Quantum Dynamics in Complex Systems. *WIREs Comput. Mol. Sci.* **2022**, 12, e1614.

(15) Tanimura, Y.; Kubo, R. Time Evolution of a Quantum System in Contact with a Nearly Gaussian-Markoffian Noise Bath. *J. Phys. Soc. Jpn.* **1989**, 58, 101–114.

(16) Ishizaki, A.; Fleming, G. R. Unified Treatment of Quantum Coherent and Incoherent Hopping Dynamics in Electronic Energy Transfer: Reduced Hierarchy Equation Approach. *J. Chem. Phys*. **2009**, 130, 234111.

(17) Kapral, R. Quantum Dynamics in Open Quantum-Classical Systems. *J. Phys.: Condens. Matter* **2015**, 27, 073201.

(18) Wang, L.; Qiu, J.; Bai, X.; Xu, J. Surface Hopping Methods for Nonadiabatic Dynamics in

Extended Systems. *WIREs Comput. Mol. Sci.* **2020**, 10, e1435.
(19) Xu, J.; Shi, Z.; Wang, L. Consistent Construction of the Density Matrix from Surface Hopping Trajectories. *J. Chem. Theory Comput.* **2024**, 20, 2349–2361.
(20) Tully, J. C. Molecular Dynamics with Electronic Transitions. *J. Chem. Phys.* **1990**, 93, 1061–1071.
(21) Fang, J.-Y.; Hammes-Schiffer, S. Improvement of the Internal Consistency in Trajectory Surface Hopping. *J. Phys. Chem. A* **1999**, 103, 9399–9407.
(22) Bittner, E. R.; Rossky, P. J. Quantum Decoherence in Mixed Quantum-classical Systems: Nonadiabatic Processes. *J. Chem. Phys.* **1995**, 103, 8130–8143.
(23) Zhu, C.; Jasper, A. W.; Truhlar, D. G. Non-Born–Oppenheimer Trajectories with Self-Consistent Decay of Mixing. *J. Chem. Phys.* **2004**, 120, 5543–5557.
(24) Shenvi, N.; Subotnik, J. E.; Yang, W. Simultaneous-Trajectory Surface Hopping: A Parameter-Free Algorithm for Implementing Decoherence in Nonadiabatic Dynamics. *J. Chem. Phys.* **2011**, 134, 144102.
(25) Guo, X.; Li, G.; Shi, Z.; Wang, L. Surface Hopping with Reliable Wave Function by Introducing Auxiliary Wave Packets to Trajectory Branching. *J. Phys. Chem. Lett.* **2024**, 15, 3345–3353.
(26) Ehrenfest, P. Bemerkung über die angenäherte Gültigkeit der klassischen Mechanik innerhalb der Quantenmechanik. *Z. Physik* **1927**, 45, 455–457.
(27) Li, G.; Shi, Z.; Guo, X.; Wang, L. What Is Missing in the Mean Field Description of Spatial Distribution of Population? Important Role of Auxiliary Wave Packets in Trajectory Branching. *J. Phys. Chem. Lett.* **2023**, 14, 9855–9863.
(28) Landry, B. R.; Falk, M. J.; Subotnik, J. E. Communication: The Correct Interpretation of Surface Hopping Trajectories: How to Calculate Electronic Properties. *J. Chem. Phys.* **2013**, 139, 211101.
(29) Guo, X.; Xu, J.; Li, G.; Wang, L. Interpretation of Adiabatic and Diabatic Populations from Trajectories of Branching Corrected Surface Hopping. *Chin. J. Chem. Phys.* **2022**, 35, 488–498.
(30) Linjun Wang; Dhara Trivedi; Oleg V. Prezhdo. Global Flux Surface Hopping Approach for Mixed Quantum-Classical Dynamics. *J. Chem. Theory Comput.* **2014**, 10, 3598–3605.
(31) Shao, C.; Xu, J.; Wang, L. Branching and Phase Corrected Surface Hopping: A Benchmark of Nonadiabatic Dynamics in Multilevel Systems. *J. Chem. Phys.* **2021**, 154, 234109.
(32) Shenvi, N.; Subotnik, J. E.; Yang, W. Phase-Corrected Surface Hopping: Correcting the Phase Evolution of the Electronic Wavefunction. *J. Chem. Phys.* **2011**, 135, 024101.
(33) Subotnik, J. E. Fewest-Switches Surface Hopping and Decoherence in Multiple Dimensions. *J. Phys. Chem. A* **2011**, 115, 12083–12096.
(34) Pieroni, C.; Agostini, F. Nonadiabatic Dynamics with Coupled Trajectories. *J. Chem. Theory Comput.* **2021**, 17, 5969–5991.
(35) Villaseco Arribas, E.; Maitra, N. T.; Agostini, F. Nonadiabatic Dynamics with Classical Trajectories: The Problem of an Initial Coherent Superposition of Electronic States. *J.Chem. Phys.* **2024**, 160, 054102.
(36) Miller, W. H. A Novel Discrete Variable Representation for Quantum Mechanical Reactive Scattering via the S-matrix Kohn Method. *J. Chem. Phys.* **1992**, 96, 1982–1991.
(37) Ishizaki, A.; Fleming, G. R. Theoretical Examination of Quantum Coherence in a

Photosynthetic System at Physiological Temperature. *PNAS.* **2009**, 106, 17255–17260.

(38) Caldeira, A. O.; Leggett, A. J. Quantum Tunnelling in a Dissipative System. *Annals of Physics* **1983**, 149, 374–456.

(39) Sun, X.; Wang, H.; Miller, W. H. Semiclassical Theory of Electronically Nonadiabatic Dynamics: Results of a Linearized Approximation to the Initial Value Representation. *J. Chem. Phys.* **1998**, 109, 7064–7074.

(40) Wang, H.; Thoss, M.; Miller, W. H. Systematic Convergence in the Dynamical Hybrid Approach for Complex Systems: A Numerically Exact Methodology. *J. Chem. Phys.* **2001**, 115, 2979–2990.